Label-free second-harmonic phase imaging of biological specimen by digital holographic microscopy

Etienne Shaffer,[1,*] Corinne Moratal,[1] Pierre Magistretti,[1] Pierre Marquet,[1,2] and Christian Depeursinge[1]

[1]*École Polytechnique Fédérale de Lausanne (EPFL), CH-1015 Lausanne, Switzerland*

[2]*Département de Psychiatrie–CHUV, Site de Cery, 1008 Prilly, Lausanne, Switzerland*

**Corresponding author: etienne.shaffer@epfl.ch*

Received August 27, 2010; revised November 5, 2010; accepted November 8, 2010; posted November 10, 2010 (Doc. ID 134136); published December 3, 2010

We have previously developed a new way for nonscanning second-harmonic generation (SHG) microscopy [Opt. Lett. **34**, 2450 (2009)]. Based on digital holography, this technique captures, in single-shot hologram acquisition, both the amplitude and the phase of a coherent SHG radiation, which makes possible second harmonic phase microscopy. In this work, we present holographic SHG phase microscopy of a label-free biological tissue and discuss its added value to SHG microscopy.

OCIS codes: 090.1995, 180.4315, 110.0180.

Second-harmonic generation (SHG) has emerged as a promising imaging technique for biological applications [1–10]. Originally developed alongside incoherent nonlinear microscopy (multiphoton excitation fluorescence), it contributed to the emergence of coherent nonlinear microscopy (e.g., higher harmonic generation, sum- or difference-frequency generation, wave mixing, coherent anti-Stokes Raman scattering). One relatively unexploited advantage of SHG—and, more generally, of coherent nonlinear microscopy—lies in its coherent nature providing both the amplitude and the phase information that can be efficiently retrieved, e.g., by means of digital holography. Indeed, holographic harmonic microscopy has recently been reported [11] and has led to quantitative exploitation of the SHG phase [12,13]. The first holographically recorded SHG intensity images of label-free biological specimens were reported this very year [14]. We report in this Letter on the first ever (to our knowledge) application of SHG phase microscopy, targeted to a label-free biological specimen. We show that the SHG phase has the potential to provide key information for better understanding of material structure, here collagen, and could lead to quantitative assessments of refractive index and/or spatial distribution of second-harmonic scatterers.

Holography consists in using a reference wave to encode the complex diffraction pattern of an object into an interference image called a hologram. Digital holograms are recorded with a digital camera and numerically reconstructed with a computer. Images numerically reconstructed from digital holograms are complex in nature and contain quantitative information on both the amplitude and the phase of the object wave [15–17]. In this work, single-shot amplitude and phase image acquisition is made possible by the off-axis holographic configuration. For details on the hologram reconstruction technique used and on its application to second-harmonic fields, see [15,18,12].

Our holographic SHG microscope (Fig. 1) is a Mach–Zehnder interferometer consisting of an object arm (**O**) and a reference arm (**R**). In **O**, the laser beam is loosely (≈30 μm FWHM) focused on the specimen. SHG occurs in the illuminated region, and the SHG object wave is collected alongside the fundamental illumination by a 63×, 0.75 NA microscope objective and imaged on the detector. In **R**, the laser beam is focused on a β-barium borate frequency doubler crystal (FDC) that generates the second-harmonic reference wave, which is then collimated, expanded, and projected on the detector, where it interferes with the object wave. An optical delay line matches the optical path length of **R** to that of **O**, ensuring that each pulse interferes with itself at the detector. The light source is a 800 nm wavelength Ti:sapphire laser, with no dispersion precompensation module, delivering >150 fs pulses at a repetition rate of 80 Mhz. The measured energy in the specimen plane is 40 nJ · pulse^{-1}. For bright-field images, the femtosecond laser was replaced by a light-emitting device, whose wavelength matches that of the SHG signal, so that the optical resolution remains the same. Polarizers on rotation mounts could be inserted before the condenser lens *C* and in the infinity space of the microscope objective for cross-polarization bright-field images. Finally, the detector, designed for fluorescence imaging, is a 12-bit CCD, with 6.45 μm pixels, working at 8.3 frames/s, with an exposure time of 120 ms. At all time, bandpass filters ensured that only light of wavelength 400 ± 20 nm reached the CCD.

Specimens consist of 5-μm-thick coronal sections of mouse tail, fixed with paraformaldehyde 4% and embedded in paraffin. Some sections were stained with

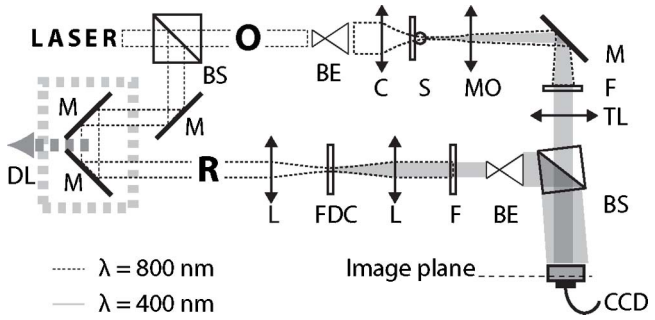

Fig. 1. Experimental setup schematics: BS, beam splitter; BE, beam expander; DL, optical delay line; C, condenser lens; S, specimen; MO, microscope objective; M, mirror; TL, tube lens; F, bandpass filter; L, lens; FDC, β-barium borate frequency doubler crystal.

histological dyes revealing collagen (Sirius Red, Goldner, and Masson Trichrome), while others were kept unstained. The purpose of stained sections is to identify collagen fibers in the dermis, while the unstained sections served for label-free SHG measurements. We chose such specimens, since it is well-known that collagen generates strong second-harmonic signals [1,5–7,9,10].

In a first step, the stained sections were examined with a bright-field microscope to identify collagen structures (e.g., collagen fibers constituting connective tissue) and then with our holographic SHG microscope to verify that collagen fibers do generate second-harmonic signals. The results, not presented in this Letter, confirmed that second harmonic was generated by the collagen fibers, as expected. In a second step, we made similar measurements on an unstained section to validate that the SHG signal did not come from the histological stains but was instead intrinsic to the specimen (Fig. 2).

While a bright-field image of the specimen [Fig. 2(a)] gives a good idea of what the specimen looks like, in terms of its geometry, it provides no way of differentiating between the materials. In comparison, a cross-polarized bright-field image of the same region [Fig. 2(b)] highlights birefringent materials by mapping the phase retardation for a given incident polarization. However, since the specimen is relatively thin (5 μm), birefringence effects remain rather weak. Finally, holographic SHG amplitude and phase images [Figs. 2(c) and 2(d)], reconstructed from the same hologram, reveal the presence of collagen. All images of Fig. 2 were recorded at the same imaging wavelength and with the same microscope objective. Therefore, fine structure seen in SHG images but not in bright-field images are not a matter of resolution but of imaging contrast and suggest that second-harmonic imaging provides specific information, impossible to retrieve with bright-field microscopy.

Right from the start, it is worth noting that the SHG amplitude is linked to the Gaussian profile of the illumination, implying that some normalization would be required before quantitative pixel-to-pixel comparisons can be made. While this drawback of nonscanning SHG microscopy could, of course, be corrected by beam homogenizing optics, it is interesting that the SHG phase [Fig. 2(d)] does not depend on the illumination intensity and, once reconstructed, can be quantitatively analyzed as is, all over the field of view. Another observation is that the phase of SHG seems to have a better signal-to-noise ratio (SNR) than its amplitude, as can be seen near the edges of the images where almost no second harmonic is generated but where the phase nevertheless reveals structures that are impossible to distinguish in amplitude contrast. Finally, it is easy to distinguish regions where no second harmonic is generated, as they result in a physically meaningless randomly distributed SHG phase. In case this disturbs the observer, one could imagine a filter, based on thresholding of the SHG amplitude, that would remove random phase fluctuations.

Where the SHG phase is defined, i.e., where SHG occurs, it is related to the phase of the fundamental wave at the location z_{SHG} of nonlinear interaction, as well as on the optical path length (at SHG wavelength) from that point to the detector. The SHG phase φ can thus be expressed in terms of refractive index n, fundamental wavelength λ, and axial coordinate z as

$$\varphi = \int_{z_I}^{z_{\mathrm{SHG}}} \frac{2\pi}{\lambda} n(z,\lambda)\mathrm{d}z + \int_{z_{\mathrm{SHG}}}^{z_F} \frac{2\pi}{\lambda/2} n(z,\lambda/2)\mathrm{d}z, \qquad (1)$$

where z_I and z_F are the coordinates of the light source and the detector, respectively. Unfortunately, the SHG phase itself is not enough to differentiate changes in the refractive index from changes in axial coordinates of SHG, for it depends on the coupled effects of both. This frustrating problem will appear somewhat familiar to the digital holographists who encountered a similar challenge in linear holography and came up with methods for decoupling refractive index and specimen thickness. Such methods include changing the known value of refractive index of the surrounding medium [19], confining the specimen in a microchannel of known depth [17], or using air bubbles in the medium surrounding the specimen to determine its refractive index [16]. Readers will therefore understand that using the SHG phase to quantitatively assess physical properties like refractive index and axial coordinates of SHG is a big challenge, beyond the scope of this Letter, that will have to be addressed in future works. It has, however, already been shown that for SHG-emitting nanoparticles located in a nondispersive medium, the SHG phase can be directly related to the axial position of the particle at a nanometer-scale precision [13].

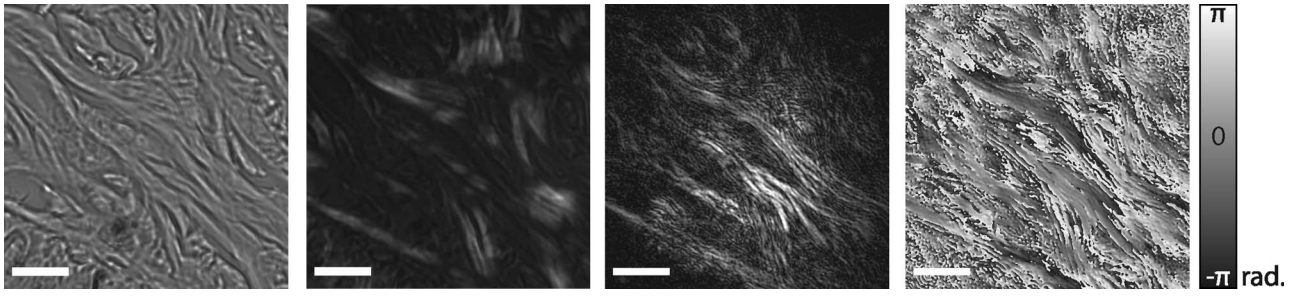

Fig. 2. Mouse tail dermis and epidermis (bottom left corner). (a) Bright field image. (b) Cross-polarization image showing phase retardation caused by the birefringence of collagen. (c), (d) SHG amplitude (normalized) and phase (wrapped) reconstructed from a single hologram. All images present the same region of the specimen and scale bars are 10 μm. Media 1, pseudocolor overlay of (b) and (c).

Even if we cannot yet relate the SHG phase to quantitative changes of physical properties, it still has a lot to offer to SHG microscopy. Reporting this year in *Chinese Optics Letters*, Xu *et al.* [10] propose a quasi-crystal model of collagen to explain the results of their polarization-based investigation of its SHG. In their work, they suggest that single molecule SHG would be too weak to account for the detected SHG signal and that coherent scattering had to play an important role. They add that a completely turbid medium would not offer the opportunity of coherent SHG scattering. The observation of the phase of the SHG signal we report here tends to support this theory. Indeed, for coherent scattering to occur, some phase-matching conditions must be satisfied. Otherwise, second harmonic generated at different depths would not add up coherently, and the SHG phase would be randomly distributed. The well-defined and continuous SHG phase of Fig. 2(d) is not compatible with such a model of single-molecule SHG in a completely turbid collagen medium and instead hints at a coherent scattering process.

Also supporting this coherent scattering process are the complementary cross-polarization [Fig. 2(b)] and holographic SHG images [Figs. 2(c) and 2(d)]—see Media 1 for overlay. Where one provides maximal contrast, the other provides almost none. We believe that this can be understood by reasoning in terms of phase matching conditions for coherent scattering. It appears that for the given incident polarization of the femtosecond laser illumination, phase matching is verified only where no retardation is observed in Fig. 2(b).

In conclusion, we have reported what we believe to be the first label-free, holographic SHG phase contrast images of biological specimen. Off-axis digital holographic microscopy is a nonscanning, single-shot image acquisition technique, limited only by the camera frame rate (and available SHG signal). It is therefore especially suited for real-time imaging and truly exploits the instantaneous response of SHG. It should be obvious that, to this day, nonscanning holographic SHG cannot compete with scanning SHG microscopy in terms of sensitivity. Holographic SHG offers coherent amplification, low sensitivity to shot noise and very high phase SNR, but, in the end, it all comes back to a matter of available light sources and detectors. Much more powerful ultrafast laser sources are needed to provide peak powers comparable to those offered by scanning microscopes but over a large field of views. In addition, very sensitive array detectors are required to compete with photomultiplier tubes. It is no wonder that the increasing enthusiasm around holographic SHG microscopy is fueled by the recent developments of both ultrafast lasers and electron-multiplying digital cameras.

The authors would like to thank Sandor Kasas for fruitful discussions. This work was financially supported in part by the Swiss National Competence Center in Biomedical Imaging (NCCBI) and by the Swiss National Science Foundation (SNSF), grant no. 205320-130543.

References

1. I. Freund and M. Deutsch, Opt. Lett. **11**, 94 (1986).
2. Y. C. Guo, P. P. Ho, H. Savage, D. Harris, P. Sacks, S. Schantz, F. Liu, N. Zhadin, and R. R. Alfano, Opt. Lett. **22**, 1323 (1997).
3. P. J. Campagnola, M. D. Wei, A. Lewis, and L. M. Loew, Biophys. J. **77**, 3341 (1999).
4. L. Moreaux, O. Sandre, M. Blanchard-Desce, and J. Mertz, Opt. Lett. **25**, 320 (2000).
5. A. Zoumi, A. Yeh, and B. J. Tromberg, Proc. Natl. Acad. Sci. USA **99**, 11014 (2002).
6. W. R. Zipfel, R. M. Williams, R. Christie, A. Y. Nikitin, B. T. Hyman, and W. W. Webb, Proc. Natl. Acad. Sci. USA **100**, 7075 (2003).
7. S. J. Lin, R. J. Wu, H. Y. Tan, W. Lo, W. C. Lin, T. H. Young, C. J. Hsu, J. S. Chen, S. H. Jee, and C. Y. Dong, Opt. Lett. **30**, 2275 (2005).
8. L. Fu, X. S. Gan, and M. Gu, Opt. Lett. **30**, 385 (2005).
9. D. Ait-Belkacem, A. Gasecka, F. Munhoz, S. Brustlein, and S. Brasselet, Opt. Express **18**, 14859 (2010).
10. P. Xu, E. Kable, C. J. R. Sheppard, and G. Cox, Chinese Optics Letters **8**, 213 (2010).
11. Y. Pu, M. Centurion, and D. Psaltis, Appl. Opt. **47**, A103 (2008).
12. E. Shaffer, N. Pavillon, J. Kühn, and C. Depeursinge, Opt. Lett. **34**, 2450 (2009).
13. E. Shaffer, P. Marquet, and C. Depeursinge, Opt. Express **18**, 17392 (2010).
14. O. Masihzadeh, P. Schlup, and R. A. Bartels, Opt. Express **18**, 9840 (2010).
15. E. Cuche, P. Marquet, and C. Depeursinge, Appl. Opt. **38**, 6994 (1999).
16. B. Kemper, D. Carl, J. Schnekenburger, I. Bredebusch, M. Schäfer, W. Domschke, and G. von Bally, J. Biomed. Opt. **11**, 034005 (2006).
17. N. Lue, G. Popescu, T. Ikeda, R. Dasari, K. Badizadegan, and M. Feld, Opt. Lett. **31**, 2759 (2006).
18. U. Schnars and W. P. O. Juptner, Meas. Sci. Technol. **13**, R85 (2002).
19. B. Rappaz, F. Charriere, C. Depeursinge, P. J. Magistretti, and P. Marquet, Opt. Lett. **33**, 744 (2008).